ACS Chemical Neuroscience

Research Article

pubs.acs.org/chemneuro

In Silico Cross Seeding of Aβ and Amylin Fibril-like Oligomers

Workalemahu M. Berhanu, Fatih Yaşar, and Ulrich H. E. Hansmann*

Department of Chemistry & Biochemistry, University of Oklahoma, Norman, Oklahoma 73019, United States

Supporting Information

ABSTRACT: Recent epidemiological data have shown that patients suffering from Type 2 Diabetes Mellitus have an increased risk to develop Alzheimer's disease and vice versa. A possible explanation is the cross-sequence interaction between Aβ and amylin. Because the resulting amyloid oligomers are difficult to probe in experiments, we investigate stability and conformational changes of Aβ−amylin heteroassemblies through molecular dynamics simulations. We find that Aβ is a good template for the growth of amylin and vice versa. We see water molecules permeate the β-strand−turn−β-strand motif pore of the oligomers, supporting a commonly accepted mechanism for toxicity of β-rich amyloid oligomers. Aiming for a better understanding of the physical mechanisms of cross-seeding and cell toxicity of amylin and Aβ aggregates, our simulations also allow us to identify targets for the rational design of inhibitors against toxic fibril-like oligomers of Aβ and amylin oligomers.

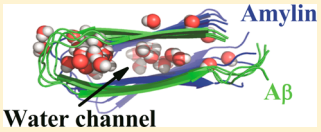

KEYWORDS: *Amyloid oligomer, water channel, molecular dynamics, crosses seeding*

Amyloid diseases are characterized by the presence of extracellular or intracellular fibrous protein deposits, known as amyloids.[1,2] While the precise nature of the toxic agents has not yet been established,[3] a likely culprit are amyloid oligomers formed from disease-specific peptides.[4,3] Common features[5,4] of such oligomers are that they are cytotoxic, recognizable by an oligomer specific antibody and rich in β-sheets. With their fibril-like morphology they can also seed new populations of oligomers.[6−8]

These commonalities in molecular structure may cause the observed correlations between amyloid diseases. For instance, patients with diabetes have an increased risk of developing Alzheimer's disease.[9,10] A controlled community-based epidemiologic and pathological study has indicated also an increased risk of type 2 diabetes in patients with Alzheimer's disease.[11] In Alzheimer disease mouse models an increased circulating Aβ level is correlated with impaired glucose/insulin tolerance and hepatic insulin resistance.[12] All these studies suggest a bidirectional relationship between type 2 diabetes and Alzheimer disease.[13] While Alzheimer's disease is characterized by the aggregation and accumulation of amyloid-β (Aβ), human amylin constitutes the major part of the pancreatic amyloid found in patients with type 2 diabetes.[14,15] One possible explanation for the link between the two diseases is cross-seeding, that is, the promotion of aggregation of one protein by another protein.

Adding a preformed template to a solution of amyloidic peptides reduces significantly the duration of lag phase in formation of amyloid oligomers. In the case of amylin$_{20-28}$ and Aβ$_{25-33}$, the large overlap (90%) in the structural properties,[11,16] which both form a U-shaped β-strand−turn−β-strand motif (Figure 1A,B), leads in vitro to formation of amyloid heteroassemblies of Aβ and amylin.[17,16] Both peptides are found in blood and cerebrospinal fluid at similar concentrations,[18,19] and a recent study found accumulations of mixed amylin and Aβ aggregates in the brain of type II diabetes and AD patients.[20] Because the prefibrillar assemblies of both amylin and Aβ destabilize synthetic phospholipid bilayers and cell membranes, one can conjecture that amyloid heteroassemblies of Aβ and amylin have similar toxic properties. This would explain the link between the two diseases.

In order to test this conjecture one needs to determine not only the structure and stability of the Aβ and amylin amyloid assemblies but also how they interact with cell membranes and other molecules. A widely accepted mechanism for the neurotoxicity[21] of amyloid oligomers is that they can form membrane or channel pores lowering the permeability barrier[22] by enabling water leakage through cell membranes. Another prominent hypothesis is that the oligomers expose hydrophobic sites that facilitate aberrant interactions and sequestration of other proteins, impairing their function.[4] Investigating such questions of structure, stability, and functions directly in experiments is difficult, but atomistic mechanisms of amyloid formation[23] and growth[24−27] can be modeled by molecular dynamics simulations and compared with experimental measurements.[28] Examples of such computational studies are recent investigations of amyloid heteroassociation between Aβ and tau fibrils. These studies suggest that the U-turn-based structural core of tau filaments promotes cross-interaction with the amyloid-β peptide, demonstrating the possibility of cross-seeding between nonhomologous proteins.[29,30] In this article, we examine the cross-seeding between amylin and Aβ, using molecular dynamics simulations on octamer oligomer of amylin, Aβ, and a mixture of both peptides (four strands from each), respectively. Our simulations test whether the U-shaped fibril model represents the molecular structure of the cross-seeded Aβ−amylin assemblies, and the role of the different structural elements of the U-shaped β-strand−

Received: July 24, 2013
Accepted: September 5, 2013
Published: September 5, 2013

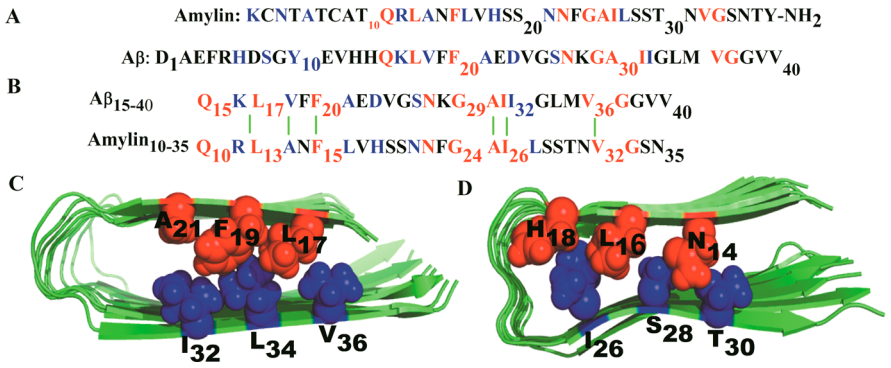

Figure 1. Sequence and structure of the amylin and Aβ_{1-40} domains involved in cross-seeding. (A) Sequences of Aβ_{1-40} and amylin. Identical residues are indicated in red and similar residues in blue.[17] (B) Domains involved in heteroassociation based on structural models of amylin[38] and Aβ fibril models.[62] The green lines illustrate hydrophobic interactions. (C) Face-to-face hydrophobic contacts between residues L_{17}/V_{36}, F_{19}/L_{34}, and A_{21}/I_{32} of Aβ and (D) Face-to-face hydrophobic contacts between residues N_{14}/T_{30}, L_{16}/S_{28}, and H_{18}/I_{26} for amylin. Residues at the N-terminus are colored red and their C-terminal partners in blue.

turn−β-strand motif for the stability and conformational dynamics of the Aβ−amylin assembly. These stability investigations are complemented by ones that probe whether water molecules can penetrate their β-strand−turn−β-strand motif pore, that is, whether Aβ−amylin assemblies can lead to water leakage through cell membranes, the commonly accepted mechanism of toxicity. While the purpose of this article is to add to a better understanding of the physical mechanism of cross-seeding between amylin and Aβ and of the mechanism for the cell toxicity of the resulting oligomers, it also points to the β_1 and β_2 regions as potential targets for the design of aggregation inhibitors.[31,32]

RESULTS AND DISCUSSIONS

Structural Stability of Self- and Cross-Seeded Oligomers. An overall picture of the conformational changes over the course of the simulation can be gained by comparing the average structures with the initial one. The average structure is calculated from the position of all heavy atoms of the protein over the 300 ns molecular dynamics trajectories using the program *g_covar* of the Gromacs 4.5.3 package. The so-calculated average structures and their C_α-RMSD (root-mean-square deviation) values with respect to the initial structures (Figure 2) show that the U-shaped conformation of the octameric oligomers is retained. Among the three octamers, amylin is the most stable system. It has the lowest C_α-RMSD, with an average ⟨RMSD⟩ in the range of 2.2−3.1 Å. Conformational drifts are observed only for the outer strands in the Aβ_{15-40} and Aβ_{15-40}|amylin$_{10-35}$ heteroassemblies leading to average ⟨RMSD⟩ of 4.3−5.1 and 4.1−5.1, respectively. This picture is supported also by average root-mean-square fluctuations calculated either for each residue or for each single strand and shown in Figure S1, Supporting Information. The residues with larger backbone root-mean-square fluctuation (RMSF) values have increased average solvent accessible surface area (SASA) values as calculated by the standard Gromacs tool *g_sas*. This suggests that they are exposed to the solvent to a larger degree (Figure 3A−C). Especially, the residues from the inner strands are less solvent-exposed than those of the more flexible outer strands. The central residues in the N terminal (residues 17−21 for Aβ and residues 12−16 for amylin) and C terminal residues (residues 30−35 for Aβ and residues 25−30 for amylin) have much smaller mean solvent exposure than edge strands; that is, they remain inaccessible

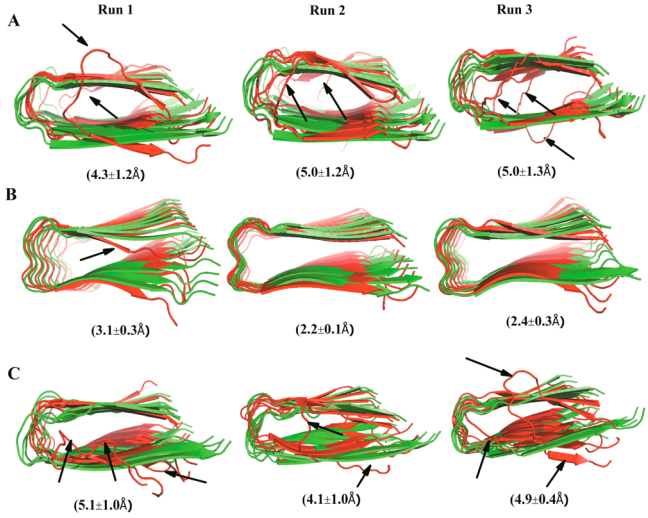

Figure 2. Average structures and C_α root-mean-square deviations (RMSDs) with respect to the corresponding minimized start configurations. Cartoon representation of the initial (green) and averaged structures (red) from three independent trajectories over 300 ns simulation of (A) Aβ_{15-40} octamers; (B) amylin$_{10-30}$ octamers; and (C) Aβ_{15-40}|amylin$_{15-35}$ octamers. Averaged RMSD values calculated for each peptide with respect to the start configurations are included in parentheses. Major differences between the average and initial structures are highlighted by black arrows pointing out the flexible edge strands.

(Figure 3A−C) to the solvent during the whole simulations. The RMSF and SASA values for the Aβ_{15-40}|amylin$_{10-35}$ heteroassemblies (Figure S1C, Supporting Information, and Figure 3C) signal that the chains at the border between amylin and Aβ change their configuration to enhance favorable interactions between them (i.e., the amylin strands at the interface have C-terminal RMSF values of about 4 Å compared with about 2 Å in the amylin octamer). This structural adjustment observed at the interface between amylin and Aβ, two peptides with different side-chain packing, is in agreement to previous experimental observation on heteroassembly of amyloid fibrils.[33,34]

Hydrogen Bond Analysis. The differences in stability between the three studied octamers result from differences in the association forces that keep them together. Especially important here are hydrogen bonds as the architecture of the

dx.doi.org/10.1021/cn400141x | ACS Chem. Neurosci. 2013, 4, 1488−1500

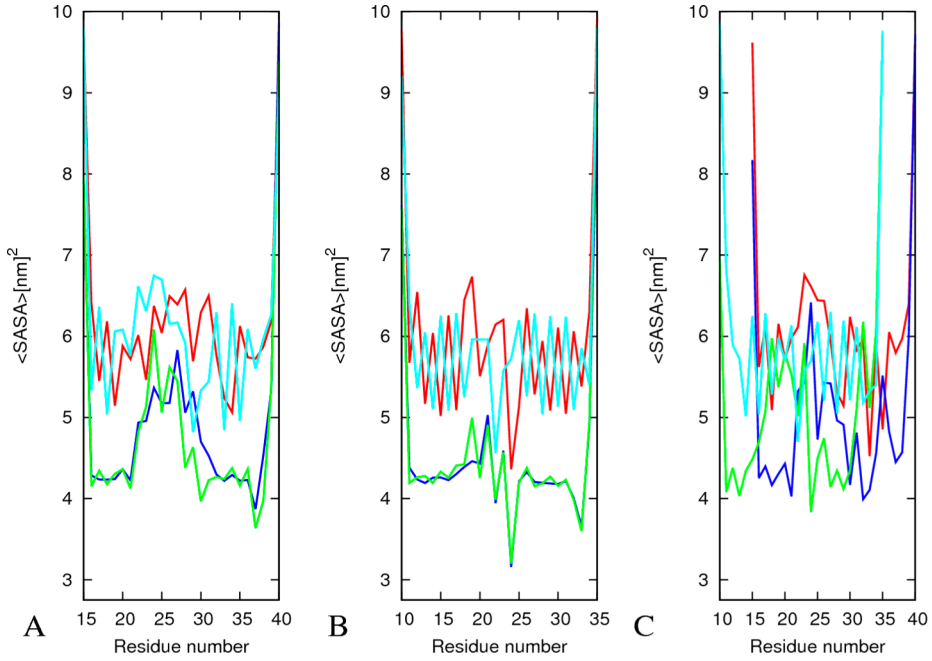

Figure 3. Average solvent accessible surface area (SASA) of the three octamers. The average SASA per strand for Aβ_{15-40} (A), amylin$_{10-35}$ (B), and Aβ_{15-40}|amylin$_{15-35}$ (C) octamers. Chain 1, red; chain 4, blue; chain 5, green; and chain 8, cyan. Chain 2, 6, and 7 have SASA values similar to chains 4 and 5, and they are not shown to simplify the figure.

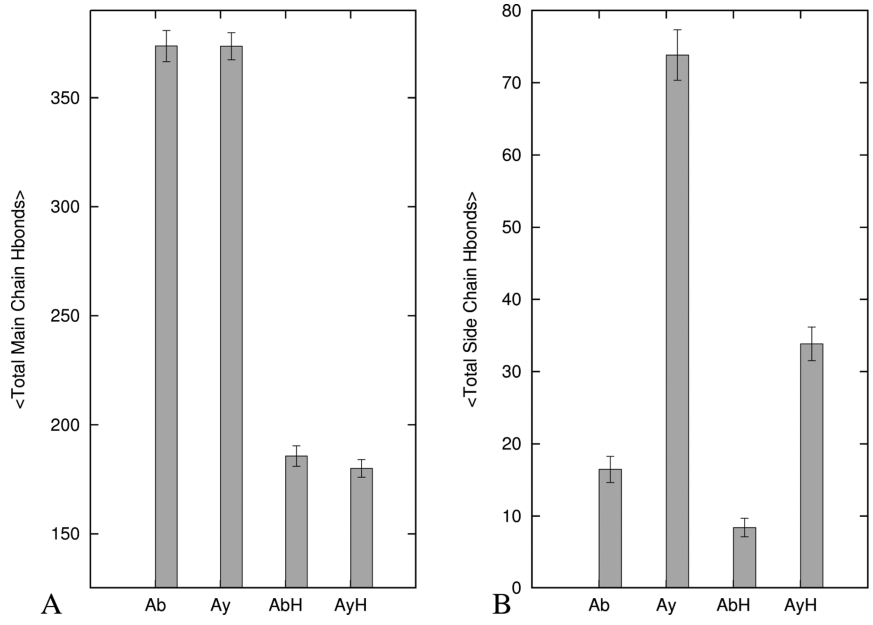

Figure 4. Average numbers of main chain and side chain hydrogen bonds in β-strand−loop−β-strand regions of the three oligomers: (A) total number of main chain hydrogen bonds; (B) total number of side chain hydrogen bonds. Legend: Ab = Aβ_{15-40}, Ay = amylin$_{10-35}$, AbH = Aβ_{15-40} part of the heteroassembly system, and AyH = amylin$_{10-35}$ part of the heteroassembly system.

amyloid fibrils dependent strongly on an array of inter backbone hydrogen bonds between the β-strands within the core of the fibril.[35,2]

The total number of hydrogen bonds (main chain and sides chains) is shown in Figure 4 for all three oligomers. The corresponding numbers for the key segments (the C terminal, loop, and N terminal regions) are shown in Supplemental Figure S2, Supporting Information. The average number of main chain to main chain hydrogen bonds in the β_1 and β_2 regions of the Aβ_{15-40}, amylin$_{10-35}$, and Aβ_{15-40}|amylin$_{10-35}$ oligomers differ little when the less stable terminal chains 1 and 8 are excluded. Because the U-shaped motif is retained in all three octamers, this indicates inter- and intramolecular main chain hydrogen bonds play a significant role in stabilizing this structure. The number of hydrogen bonds per residue is smaller in the loop region than in the β regions making this region more flexible and less stable (Figure S2, Supporting Information). Aβ_{15-40} lacks side chain to side chain hydrogen bonds in both β regions while in amylin$_{10-35}$ such side chain to side chain hydrogen bonds help to retain the U-shaped geometry of the amylin oligomer. While the total number of main chain to main chain hydrogen bonds (which is directly

dx.doi.org/10.1021/cn400141x | ACS Chem. Neurosci. 2013, 4, 1488−1500

Table 1. Average Hydrophobic Contact Distances between Selected Adjacent Hydrophobic Residues of $A\beta_{15-40}$, $Amylin_{15-35}$ and Their Cross-Seeded Oligomers ($A\beta_{15-40}$|$Amylin_{15-35}$)

	Aβ oligomer				Aβ oligomer				Aβ oligomer		
F_{20}/F_{20}[a] contacts	run 1	run 2	run 3	I_{32}/I_{32}[a] contacts	run 1	run 2	run 3	V_{36}/V_{36}[a] contacts	run 1	run 2	run 3
chains 2−3	4.95(0.2)	4.97(0.2)	5.30(0.7)	chains 2−3	4.79(0.3)	5.40(0.6)	4.92(0.3)	chains 2−3	4.99(0.5)	4.81(0.2)	4.80(0.2)
chains 3−4	4.93(0.2)	4.96(0.3)	4.92(0.3)	chains 3−4	4.82(0.2)	5.24(0.3)	5.28(0.9)	chains 3−4	4.77(0.2)	4.78(0.2)	4.77(0.2)
chains 4−5	4.91(0.2)	4.95(0.2)	4.92(0.2)	chains 4−5	4.81(0.1)	4.81(0.2)	4.73(0.8)	chains 4−5	4.99(0.4)	4.82(0.2)	4.80(0.2)
chains 5−6	4.93(0.2)	4.92(0.2)	4.97(0.2)	chains 5−6	4.96(0.3)	4.83(0.2)	4.77(0.1)	chains 5−6	5.22(0.2)	4.85(0.2)	4.76(0.1)
chains 6−7	4.82(0.2)	4.97(0.3)	4.96(0.3)	chains 6−7	6.38(1.6)	4.99(0.2)	4.91(0.2)	chains 6−7	5.10(0.2)	4.82(0.2)	4.90(0.2)
mean ± SD	4.91 ± 0.05	4.95 ± 0.02	5.01 ± 0.2	mean ± SD	5.15 ± 0.7	5.05 ± 0.3	4.92 ± 0.2	mean ± SD	11.1 ± 0.52	1.59 ± 0.8	11.09 ± 0.4
	amylin oligomer				amylin oligomer				amylin oligomer		
F_{15}/F_{15}[a] contacts	run 1	run 2	run 3	I_{26}/I_{26}[a] contacts	run 1	run 2	run 3	V_{32}/V_{32}[a] contacts	run 1	run 2	run 3
chains 2−3	4.82(0.2)	4.81(0.2)	4.82(0.2)	chains 2−3	4.79(0.2)	4.78(0.2)	4.77(0.2)	chains 2−3	5.24(0.4)	4.77(0.2)	4.86(0.2)
chains 3−4	4.75(0.2)	4.79(0.2)	4.83(0.2)	chains 3−4	4.80(0.2)	4.81(0.2)	4.89(0.2)	chains 3−4	4.99(0.3)	4.70(0.1)	4.81(0.2)
chains 4−5	4.79(0.2)	4.81(0.2)	4.86(0.2)	chains 4−5	4.88(0.2)	4.91(0.2)	4.94(0.2)	chains 4−5	4.95(0.2)	4.70(0.2)	4.75(0.2)
chains 5−6	4.83(0.2)	4.79(0.2)	4.94(0.2)	chains 5−6	4.79(0.2)	4.89(0.2)	4.79(0.2)	chains 5−6	4.78(0.2)	4.73(0.2)	4.86(0.2)
chains 6−7	4.81(0.2)	4.81(0.2)	4.82(0.2)	chains 6−7	4.86(0.2)	4.91(0.2)	4.77(0.2)	chains 6−7	4.89(0.2)	4.76(0.2)	4.74(0.2)
mean ± SD	4.80 ± 0.03	4.80 ± 0.01	4.80 ± 0.05	mean ± SD	4.82 ± 0.04	4.86 ± 0.06	4.83 ± 0.08	mean ± SD	4.97 ± 0.2	4.73 ± 0.03	4.80 ± 0.06
	Aβ−amylin heteroassembly				Aβ−amylin heteroassembly, Aβ				Aβ−amylin heteroassembly, Aβ		
F/F[a] contacts	run 1	run 2	run 3	I/I[a] contacts	run 1	run 2	run 3	V/V[a] contacts	run 1	run 2	run 3
chains 2−3 (Aβ)	4.82(0.2)	4.89(0.2)	4.79(0.2)	chains 2−3 (Aβ)	5.02(0.2)	4.81(0.2)	4.86(0.2)	chains 2−3 (Aβ)	5.32(0.7)	5.07(0.3)	4.89(0.2)
chains 3−4(Aβ)	4.81(0.2)	5.14(0.3)	4.81(0.2)	chains 3−4(Aβ)	4.96(0.2)	5.26(0.2)	4.95(0.2)	chains 3−4(Aβ)	7.90(2.4)	4.90(0.3)	4.82(0.2)
chains 4−5	4.89(0.2)	4.98(0.2)	5.07(0.2)	chains 4−5	6.61(0.5)	6.57(0.3)	6.61(0.4)	chains 4−5	8.87(2.4)	6.79(0.6)	7.65(0.9)
chains 5−6 (amy.)	4.88(0.2)	4.92(0.2)	4.84(0.2)	chains 5−6 (amy.)	5.09(0.4)	4.95(0.2)	5.16(0.2)	chains 5−6 (amy.)	5.13(0.2)	5.03(0.3)	4.94(0.3)
chains 6−7(amy.)	4.92(0.2)	4.94(0.2)	4.82(0.2)	chains 6−7(amy.)	5.22(0.4)	5.09(0.3)	4.99(0.4)	chains 6−7(amy.)	5.51(1.1)	4.88(0.2)	4.74(0.2)
mean ± SD	4.86 ± 0.05	4.97 ± 0.1	4.87 ± 0.1	mean ± SD	5.38 ± 07	5.34 ± 0.8	5.31 ± 0.7	mean ± SD	6.55 ± 1.7	5.33 ± 0.8	5.41 ± 1.3

[a]Hydrophobic contact of $C_\alpha-C_\alpha$ distances (Å) between the residues F_{20}/F_{20}, I_{32}/I_{32}, and V_{36}/V_{36} of Aβ and F_{15}/F_{15}, I_{26}/I_{26}, and V_{32}/V_{32} of amylin and their heteroassembly. Values are shown after excluding peptides chains 1 and 8.

dx.doi.org/10.1021/cn400141x | ACS Chem. Neurosci. 2013, 4, 1488−1500

Table 2. Face-to-Face Hydrophobic Contact Distances of Aβ$_{15-40}$, Amylin$_{15-35}$ and Their Cross-Seeded Oligomers (Aβ$_{15-40}$|Amylin$_{15-35}$)

	Aβ oligomer				Aβ oligomer				Aβ oligomer		
L_{17}/V_{36}[a] contacts	run 1	run 2	run 3	F_{19}/L_{34}[a] contacts	run 1	run 2	run 3	A_{21}/I_{32}[a] contacts	run 1	run 2	run 3
chain 2	9.4(0.7)	9.2(0.6)	9.8(1.0)	chain 2	10.9(0.9)	11.2(0.6)	10.9(0.8)	chain 2	10.7(0.9)	13.2(0.7)	10.8(1.3)
chain 3	8.6(0.7)	8.1(0.6)	9.6(0.6)	chain 3	10.3(0.5)	10.5(0.5)	10.5(0.8)	chain 3	10.8(0.5)	10.5(0.7)	10.6(0.8)
chain 4	8.1(1.2)	7.4(0.7)	9.0(0.6)	chain 4	10.0(0.5)	10.3(0.5)	10.3(0.5)	chain 4	11.5(0.6)	11.3(0.6)	11.1(0.6)
chain 5	6.7(0.3)	7.1(0.6)	7.9(0.6)	chain 5	9.4(0.4)	9.8(0.5)	10.1(0.5)	chain 5	11.9(0.6)	11.6(0.6)	11.6(0.5)
chain 6	7.1(0.4)	6.9(0.3)	6.9(0.3)	chain 6	9.3(0.5)	9.3(0.4)	9.5(0.4)	chain 6	11.7(0.6)	11.5(0.6)	11.6(0.5)
chain 7	9.1(0.7)	6.9(0.4)	7.1(0.5)	chain 7	10.5(0.7)	9.2(0.4)	9.3(0.6)	chain 7	11.9(0.9)	11.4(0.6)	10.9(0.7)
mean ± SD	8.1 ± 1.1	7.6 ± 0.9	8.4 ± 1.3	mean ± SD	10.1 ± 0.2	10.1 ± 0.8	10.1 ± 0.6	mean ± SD	11.4 ± 0.5	11.6 ± 0.9	11.1 ± 0.4
	amylin oligomer				amylin oligomer				amylin oligomer		
N_{14}/T_{30}[a] contacts	run 1	run 2	run 3	L_{16}/S_{28}[a] contacts	run 1	run 2	run 3	H_{18}/I_{26}[a] contacts	run 1	run 2	run 3
chain 2	7.3(0.4)	7.8(0.4)	6.4(0.2)	chain 2	8.1(0.4)	9.1(0.4)	6.8(0.2)	chain 2	8.8(0.5)	8.8(0.4)	8.8(0.3)
chain 3	7.5(0.5)	8.0(0.4)	6.4(0.2)	chain 3	8.6(0.5)	9.2(0.4)	6.7(0.2)	chain 3	8.5(0.5)	8.8(0.4)	9.2(0.3)
chain 4	7.7(0.5)	7.9(0.3)	6.5(0.3)	chain 4	8.9(0.6)	9.1(0.4)	7.0(0.4)	chain 4	8.8(0.5)	8.9(0.4)	9.0(0.3)
chain 5	7.6(0.4)	8.0(0.3)	6.9(0.4)	chain 5	9.3(0.6)	9.0(0.4)	7.2(0.5)	chain 5	9.6(0.7)	8.7(0.4)	8.8(0.3)
chain 6	7.6(0.4)	7.8(0.4)	6.4(0.4)	chain 6	9.8(0.7)	9.0(0.5)	7.0(0.5)	chain 6	10.1(0.7)	8.6(0.6)	9.1(0.3)
chain 7	7.7(0.4)	7.7(0.4)	6.4(0.5)	chain 7	10.6(0.5)	9.1(0.8)	7.2(0.8)	chain 7	9.8(0.6)	8.9(0.7)	9.0(0.4)
mean ± SD	7.6 ± 0.1	7.9 ± 0.1	6.5 ± 0.2	mean ± SD	9.3 ± 0.9	9.1 ± 0.1	7.0 ± 0.2	mean ± SD	9.3 ± 0.6	8.8 ± 0.1	9.0 ± 0.2
	Aβ−amylin heteroassembly, Aβ				Aβ−amylin heteroassembly, Aβ				Aβ−amylin heteroassembly, Aβ		
L_{17}/V_{36}[a] contacts	run 1	run 2	run 3	F_{19}/L_{34}[a] contacts	run 1	run 2	run 3	A_{21}/I_{32}[a] contacts	run 1	run 2	run 3
chain 2	12.1(0.7)	11.2(0.5)	11.4(0.4)	chain 2	10.5(1.2)	10.3(1.1)	11.7(0.9)	chain 2	10.4(0.9)	11.5(0.7)	10.1(0.8)
chain 3	10.8(0.5)	11.9(0.7)	9.8(0.4)	chain 3	9.3(0.4)	9.7(0.6)	10.5(0.6)	chain 3	11.3(0.5)	11.8(0.5)	10.2(0.7)
chain 4	6.1(0.3)	8.2(0.7)	6.0(0.3)	chain 4	9.4(0.4)	9.4(0.5)	9.2(0.5)	chain 4	11.3(0.6)	11.4(0.5)	10.8(0.5)
mean ± SD	9.7 ± 3.2	10.4 ± 2.0	9.1 ± 2.75	mean ± SD	9.6 ± 0.4	9.8 ± 0.5	10.5 ± 1.3	mean ± SD	11.0 ± 0.5	11.6 ± 0.2	10.4 ± 0.4
	Aβ−amylin heteroassembly, amylin				Aβ−amylin heteroassembly, amylin				Aβ−amylin heteroassembly, amylin		
N_{14}/T_{30}[a] contacts	run 1	run 2	run 3	L_{16}/S_{28}[a] contacts	run 1	run 2	run 3	H_{18}/I_{26}[a] contacts	run 1	run 2	run 3
chain 5	10.6(0.8)	10.1(0.7)	9.4(0.4)	chain 5	12.1(0.7)	11.2(0.5)	11.4(0.4)	chain 5	10.0(0.6)	7.1(0.40)	9.3(0.6)
chain 6	7.7(0.4)	9.0(0.5)	7.6(0.6)	chain 6	10.8(0.5)	11.9(0.7)	9.8(0.4)	chain 6	8.6(0.5)	10.2(0.5)	8.8(0.4)
chain 7	6.4(0.3)	8.3(0.4)	6.4(0.3)	chain 7	6.1(0.3)	8.2(0.7)	6.0(0.3)	chain 7	8.6(0.4)	9.3(0.6)	8.7(0.4)
mean ± SD	8.2 ± 2.1	9.2 ± 0.9	7.8 ± 1.5	mean ± SD	9.6 ± 3.2	10.4 ± 1.9	9.1 ± 2.7	mean ± SD	9.1 ± 0.8	8.9 ± 1.6	8.9 ± 0.3

[a]Hydrophobic contact of C_α- C_α distances (Å) between the residues L_{17}/V_{36}, F_{19}/L_{34} and A_{21}/I_{32} of Aβ and N_{14}/T_{30}, L_{16}/S_{28} and H_{18}/I_{26} of amylin and their heteroassembly. Values are shown after excluding peptides chains 1 and 8.

related to in-register hydrogen bonds) is similar in all the three systems, the total number of side chain to side chain hydrogen bonds is larger in amylin$_{10-35}$ than for both Aβ$_{15-40}$ and Aβ$_{15-40}$|amylin$_{10-35}$. Hence, the lack of strong side chain hydrogen bonds in Aβ$_{15-40}$ and Aβ$_{15-40}$|amylin$_{10-35}$ and their presence in amylin$_{10-35}$ indicate that such side chain hydrogen bonds contribute to the better retention of the U-shaped geometry in amylin$_{10-35}$, as has been reported previously.[36]

Hydrophobic Interactions and Oligomer Stability. Besides hydrogen bonds, the U-shaped conformations of amylin[37,38] and Aβ[39,32] are stabilized by interpeptide hydrophobic interactions of hydrophobic residues. For this reason, we have also monitored for the three octamers the interpeptide hydrophobic interactions between adjacent residues in the $L_{13}ANFL_{17}$ and $A_{25}ILSS_{29}$ region of amylin and those in the hydrophobic residues $L_{17}VFFA_{21}$ and $A_{30}IIGL_{34}$ in Aβ. Measurements of solvent accessible surface area and root-mean-square fluctuations (Figure 3 and Figure S1, Supporting Information) show that these regions are more stable than the other parts. The hydrophobic contacts between selected adjacent residues in these hydrophobic regions are shown in Table 1. The interstrand hydrophobic side chain contacts for Aβ$_{15-40}$ are measured between F_{20} and F_{20}, I_{32} and I_{32}, and V_{36} and V_{36} of each strand and the adjacent successive once. In the case of amylin, the distances between F_{15} and F_{15}, I_{26} and I_{26}, and V_{32} and V_{32} are measured. Correspondingly, in the Aβ$_{15-40}$|amylin$_{10-35}$ oligomer, it is measured based on a combination of the above interactions. The hydrophobic phenylalanine, isoleucine, and valine interstrand contacts are retained in the simulation of the core of both the Aβ$_{15-40}$ and amylin$_{10-35}$ octamers, with distances ranging from 4.5 to 5 Å, close to the experimental results of 4.8 Å for amyloid fibrils[32] and oligomers.[6,32]

The F_{15}−F_{15}, F_{15}−F_{20}, and F_{20}−F_{20} residues (Table 1) in the β_1 regions of the Aβ$_{15-40}$|amylin$_{10-35}$ oligomer are within 4.5 to 5 Å of each other. This includes the F_{15}−F_{20} contacts at the interface between amylin and Aβ. A similar result is also observed for adjacent I_{26}−I_{26}, I_{32}−I_{32}, V_{32}−V_{32}, and V_{36}−V_{36} residues within β_2 regions. On the other hand, the hydrophobic contacts between adjacent I_{26}−I_{32} and V_{32}−V_{36} residues at the interface between Aβ and amylin (where there is a larger degree of sequence dissimilarity) in the β_2 regions of Aβ$_{15-40}$|

Table 3. The Binding Energy of Tetramer-to-Tetramer Interactions of the Octameric Oligomers and Contributions of Solvation, van der Waals, and Electrostatic Interactions Using the Single Trajectory MM-PBSA Method[a]

		$\langle\Delta E_{vdw}\rangle$	$\langle\Delta E_{ele}\rangle$	$\langle\Delta G_{PB}\rangle$	$\langle\Delta G_{SA}\rangle$	$\langle\Delta G_{solv}\rangle$	$\langle\Delta G_{binding}\rangle$
$A\beta_{15-40}$	traj 1	−135.4	−24.6	43.1	−11.2	31.8	−128.3
	traj 2	−126.4	−39.9	49.9	−10.9	38.9	−127.3
	traj 3	−130.3	−48.6	60.0	−11.4	48.7	−130.2
	traj 4	−132.6	−62.5	67.6	−11.3	56.3	−138.8
	mean value[b]	−131.2	−43.9	55.1	−11.2	43.9	−131.1
	SD[c]	3.8	15.9	10.9	0.2	10.8	5.3
$amylin_{15-30}$	traj 1	−140.1	126.1	−104.6	−10.9	−115.6	−129.6
	traj 2	−138.2	144.8	−119.6	−10.9	−130.5	−123.5
	traj 3	−140.5	135.9	−111.5	−11.1	−122.5	−127.1
	traj 4	−141.2	146.9	−123.3	−10.8	−134.1	−128.4
	mean value[b]	−140.0	138.4	−114.7	−10.9	−125.7	−127.2
	SD[c]	1.1	8.21	7.2	0.1	7.2	2.3
$A\beta_{15-40}$|$amylin_{15-30}$	traj 1	−122.7	−15.4	59.5	−10.5	46.9	−91.1
	traj 2	−122.6	−23.7	68.4	−10.5	57.9	−88.3
	traj 3	−135.5	−35.6	82.7	−11.2	71.4	−99.7
	traj 4	−122.3	−37.6	83.2	−10.9	72.2	−87.7
	mean value[b]	−125.8	−28.1	73.4	−10.8	62.1	−91.7
	SD[c]	6.5	10.4	11.6	0.4	12.1	5.5

[a] ΔE_{ele}, non-solvent electrostatic potential energy; ΔG_{PB}, electrostatic contributions to the solvation free energy calculated with Poisson−Boltzmann equation; G_{SA}, nonpolar contributions to solvation free energy; ΔE_{vdw}, van der Waals potential energy; $\Delta G_{binding}$, calculated binding, and ΔG_{solv} are total solvation energies. Data are shown as mean with the standard deviation (SD) in brackets. $\Delta G_{binding} = \Delta E_{vdw} + \Delta E_{ele} + \Delta G_{solv}$; $\Delta G_{solv} = \Delta G_{PB} + \Delta G_{SA}$. [b] Mean values are calculated from the four trajectories for each model resulting from two independent simulations. [c] The standard deviation (SD) therefore describes the deviation between the four independent simulations. Results are averages over four MD runs.

$amylin_{10-35}$ oligomer are larger than the expected distance of about 5 Å. The average distance between such pairs of residues is more than 6.5 and 7 Å, respectively. These distances suggests that a combination of stable hydrophobic contacts in the β_1 regions and a more flexible hydrophobic contact in the β_2 regions is necessary to accommodate side-chain packing between the two peptides in the heteroassemblies.

Face-to-Face Hydrophobic Contacts Inside the Interior of the Oligomers. Face-to-face interactions between β-sheets are common in proteins and amyloids. They involve hydrophobic surfaces with good shape complementarity that are held together through van der Waals and hydrophobic interactions. Such hydrophobic contacts often involve large, branched, nonpolar side chains of valine, leucine, isoleucine, and phenylalanine, because they can provide large hydrophobic areas that maximize interactions. However, polar residues such as tyrosine, tryptophan, serine, and threonine can also participate.[40] For this reason, we have monitored the hydrophobic contact between residues V_{36}/L_{17}, L_{34}/F_{19}, and I_{32}/A_{21} of Aβ and T_{30}/N_{14}, S_{28}/L_{16}, and I_{26}/H_{18} for amylin (Figure 1C,D). These contacts are calculated also in the heteroassembly, and the results are shown in Table 2. After excluding the terminal strands, the average distances between the two β-sheets within the β_1 and β_2 regions of oligomers are within 7.5 to 11 Å (Table 2). These distances are measured between the residues involved in the face-to-face hydrophobic contacts and are in agreement with experimental results, 8−11 Å.[41] Hence, in all three oligomers, the core and the β-strand−turn−β-strand motif are stabilized by such face-to-face hydrophobic interactions. The distance between the two β-sheets is about 10 Å for the Aβ octamer, while in amylin the distances are smaller by 1−2 Å. However, in the cross-seeded $A\beta_{15-40}$|$amylin_{10-35}$ octamers, the amylin strand at the interface between Aβ and amylin chains has face-to-face hydrophobic distances of 10 Å indicating that at the interface the interaction of Aβ and amylin chains requires structural flexibility and conformational adaptation for better shape complementary.

Salt Bridge Analysis for the Aβ Self-Seeding and Its Cross-Seeding with Amylin. It has been proposed that the loop region connecting the two β-sheets of the U turn or (β arch) model of Aβ are stabilized by a salt bridge between D_{23} and K_{28}[42,32] that prevents larger backbone motions. Hence, we also probe the effect of the salt bridge on the stability of the aggregates on the Aβ and its hetero-octamer assemblies. The salt bridge distance is calculated as the averaged distance of the C═O bonds of the carboxyl group of D_{23} to the N atom of the NH_3^+ in K_{28} of the intrachain salt bridge (D_{23}^n/K_{28}^n) or the interchain salt−bridge (D_{23}^n/K_{28}^{n+1}) as the carboxylate group of D_{23}^n dynamically relocates between the amine groups of adjacent K_{28}^n or K_{28}^{n+1} residues.[32,43] In agreement with previous simulations of the pentamer $A\beta_{15-40}$,[32] we observe that the $A\beta_{15-40}$ octamers form more stable interchain salt bridges than intrachain salt bridges. Note that the edge peptides at the ends of the oligomer are excluded, because they are highly flexible. The interchain and intrachain salt bridge in the $A\beta_{15-40}$|$amylin_{15-35}$ heteroassembly from the $A\beta_{15-40}$ tetramer portion also forms a stable inner salt bridge, with strong intrachain salt bridge (Figure S3, Supporting Information). Hence, the presence of these salt bridges is important for stabilizing the hydration cavity not only of the $A\beta_{15-40}$ octamers but also of the cross-seeded $A\beta_{15-40}$|$amylin_{15-30}$ heteroassembly.

The MM-PBSA Binding Free Energies for Tetramer-Tetramer Association. The binding free energy between the two tetramers for the octameric oligomers is calculated according to the thermodynamic cycle shown in Figure S4, Supporting Information, using the MM-PBSA approach.[11,28] This approach is computationally less expensive than thermodynamic integration or free energy perturbation methods because it evaluates only the bound and unbound states.[44] However, because the approach does not take into

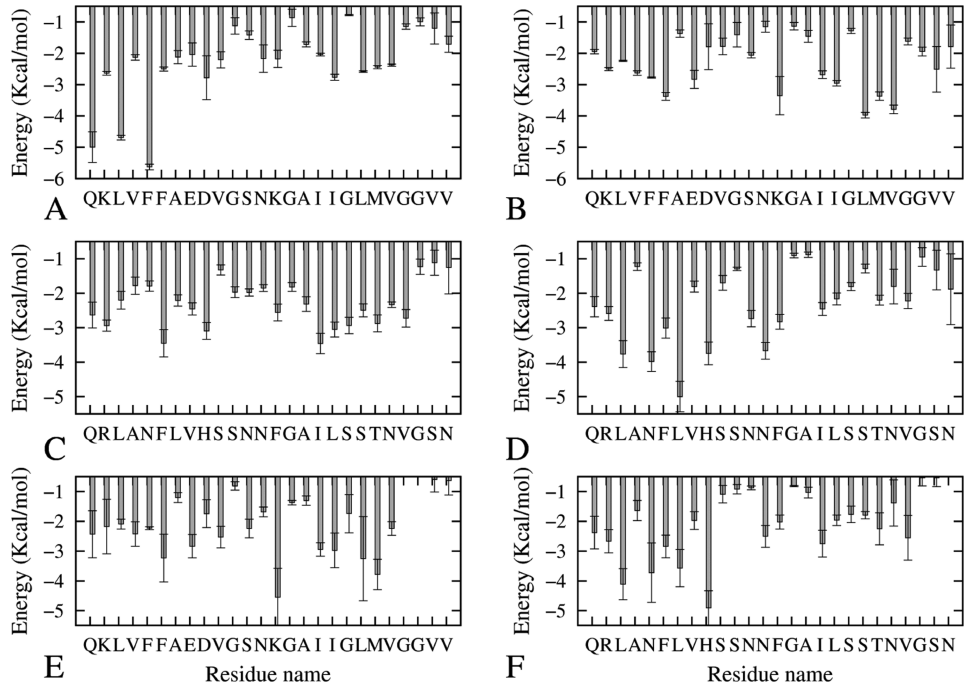

Figure 5. van der Waals contributions to the binding free energy from interactions between the interface strands in each of the three oligomers: (A) strand 4 of Aβ_{15-40}; (B) strand 5 of Aβ_{15-40}; (C) strand 4 of amylin$_{15-35}$; (D) strand 5 of amylin$_{15-35}$; (E) strand 4 (Aβ_{15-40}) of Aβ_{15-40}|amylin$_{15-35}$; (F) strand 4 (amylin$_{15-35}$) of Aβ_{15-40}|amylin$_{15-35}$.

account explicitly water and ions but models their effects by a continuum approach, its application is limited to systems without high charges where screening by water and ions is less critical. Furthermore, entropic contributions due to the release or trapping of water or ions are neglected in this approach. Despite these and other limitations, MM-PBSA, can yield reasonable approximations of relative binding energies for protein-to-protein association.[45,46] In our case, we generate 1250 equally spaced snapshots of each complex (every 40 ps) from the molecular dynamics trajectories, and all water molecules and counterions were removed before MM-PBSA calculations with the MMPBSA.py script in AMBER11. The solute entropic contributions ($T\Delta S$) have not been calculated since they cannot be estimated sufficiently accurately and their contribution to the total energy difference is small compared with the term that results from conformational changes.[47,48]

The total binding free energy for all three octamers is negative, that is, favors the stability of the aggregates over that of separated tetramers. We have listed in Table 3 both the total binding energies and their components. This separation into components can help us to understand the contributions of electrostatic, van der Waals, polar, and nonpolar interactions in stabilizing of oligomers. The electrostatic energy of Aβ_{15-40} and Aβ_{15-40}|amylin$_{10-35}$ oligomers is negative and favors the stability of the complex, but it is positive and therefore destabilizing for the amylin$_{10-35}$ octamer. Absolute values of the van der Waals interaction are larger than the electrostatic contributions, and negative for all three systems. Hence, the van der Waals interaction contribution to the stability of the oligomers is significantly favorable. The nonpolar solvation contributions also favor the octamer in all three cases; however, the larger polar solvation energy turns the total solvation energy of the Aβ_{15-40} and Aβ_{15-40}|amylin$_{10-35}$ octamers positive, that is, destabilizes them, while it is negative and stabilizing for the amylin$_{10-35}$ complex.

A decomposition of the free energies according to residues points to several amino acids as key contributors to the overall binding energy. Figure 5 and Figure S5, Supporting Information, display the residues that make significant favorable or unfavorable contributions to the van der Waals and electrostatic binding free energy of the two monomers at strands 4 and 5 of the octamers. The residues with the most favorable van der Waals interaction contributions to the binding free energy between the two chains are in the β_1 and β_2 regions (that is, $L_{13}ANFL_{17}$ in the β_1 region and $A_{25}ILSS_{29}$ in β_2 region of amylin, $L_{17}VFFA_{21}$ in the β_1 region and $A_{30}IIGL_{34}$ in the β_2 region in Aβ, and $L_{13}ANFL_{17}$ in the β_1 region and $A_{25}ILSS_{29}$ in in the β_2 region of amylin and $L_{17}VFFA_{21}$ in the β_1 region and $A_{30}IIGL_{34}$ in the β_2 region in Aβ of the Aβ−amylin heteroassembly). This observation agrees with the hydrogen bond network and hydrophobic contacts observed in Figure 4 and Table 1. Note also that the charged residues involved in the salt bridge in Aβ_{15-40} and Aβ_{15-40}|amylin$_{10-35}$ heteroassemblies (D_{24}−K_{28} and E_{23}−K_{28}) contribute favorably to the backbone and side-chain van der Waals term in the binding free energy.

The total per residue decomposition of electrostatic interaction for strands 4 and 5 of the octamers is shown in Figure S5, Supporting Information. Residues that contribute most to the electrostatic interaction in Aβ_{15-40} include the charged residues Q_{15}, K_{16}, E_{23}, D_{24}, and K_{28}. The E_{23} and D_{24} residues involved in salt bridge with K_{28} have an electrostatic interaction opposite to the contribution of K_{28}, which has been observed also in previous simulations.[49] The neighboring K_{16} disfavors oligomerization because of the unfavorable vicinity to the positively charged side chain amino groups, but the major unfavorable per residue electrostatic interaction in amylin oligomers is from R_{11}. The adjacent positively charged side chain amino leads to a positive electrostatic interaction term for the tetramer-to-tetramer binding energy term of amylin (see Table 3). This unfavorable electrostatic contribution of the R_{11}

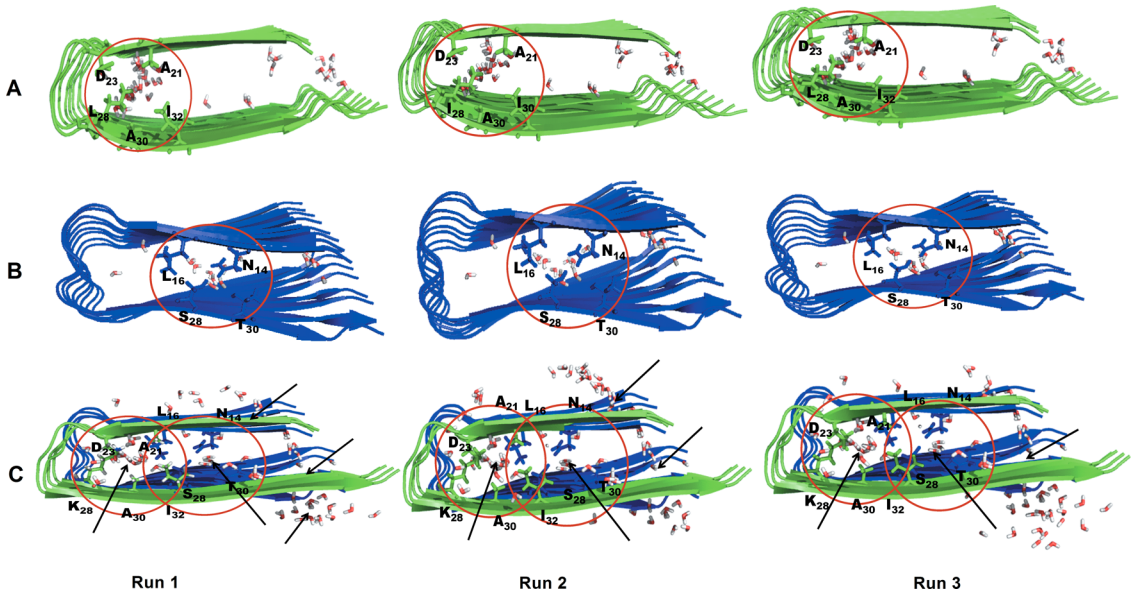

Figure 6. Snapshots of water molecules in the interior hydration cavity of the start octamer configurations: (A) $A\beta_{15-40}$, (B) $amylin_{15-35}$, and (C) $A\beta_{15-40}|amylin_{15-35}$). The water molecules are white and red colored. Residues that interact with water molecules in $A\beta_{15-40}$ (panel A, between D_{23} and K_{28} shown within the circle in blue stick representation), $amylin_{15-35}$ (panel B, between N_{14}, S_{28}, and T_{30} shown within the circle in blue stick representation), and $A\beta_{15-40}|amylin_{15-35}$ cross-seeding (panel C, between D23 and K28 for $A\beta_{15-40}$ and between N_{14}, S_{28}, and T_{30} shown within the circle in stick for $amylin_{15-35}$) are indicated.

from the amylin strand is suppressed at the interface of the $A\beta_{15-40}|amylin_{10-35}$ heteroassembly (see Figure S5, Supporting Information) leading to an overall negative electrostatic interaction term for the tetramer-to-tetramer binding energy term of amylin (see Table 3).

The binding free energy of $A\beta_{15-40}$, $amylin_{10-35}$, and $A\beta_{15-40}|amylin_{10-35}$ heteroassemblies over the constituting tetramers indicates that the nonpolar electrostatic and van der Waals terms are favorable. On the other hand, the intermolecular electrostatic and the electrostatic solvation terms cancel each other and contribute little to the association of the three oligomer systems. The per-residue energy decomposition of the nonpolar van der Waals interactions shows that the stabilizing contributions come from hydrophobic residues that are involved in the face-to-face intrastrand and interstrand interactions of all three oligomers (i.e., L_{17}, F_{19}, F_{20}, I_{32}, I_{34}, and V_{36} in $A\beta_{15-40}$; N_{14}, F_{15}, L_{16}, L_{17}, H_{18}, I_{26}, S_{28}, T_{30} and V_{32} in $amylin_{10-35}$; combination of these key amino acids in the $A\beta_{15-40}|amylin_{10-35}$ heteroassembly) through nonpolar contacts between main chains and side chains.

Interior Water Channels of the Octameric Oligomers and Toxicity. All three octamer oligomer simulations start without waters molecules inside the β-strand−turn−β-strand motif. However, during the course of the simulation, we observe that water molecules permeate the interior of the complexes. A snapshot from an early part of the production simulation illustrates that water molecules quickly and deeply penetrate into the interior of the oligomers (Figure 6). This points to water leakage through cell membranes as the cause for toxicity of β-rich amyloid oligomers. Note that our results here differ from previous studies of infinitely long fibrils where water molecules were absent in the interior. The difference is likely due to the slow equilibration between interior water and the bulk phase[43,50] because in molecular dynamics simulations of finite $A\beta$ fibril segments, internal water molecules were also present.[43,51]

The number of water molecules inside the β-strand−turn−β-strand motif pore of the oligomers is plotted in Figure 7 over

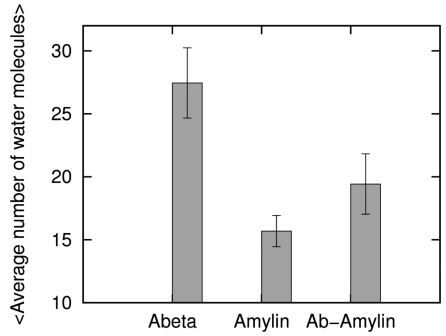

Figure 7. Time-averaged numbers of internal water molecules. Average number of water molecules in the inner cavity of (Abeta) $A\beta_{15-40}$, (Amylin) $amylin_{10-35}$, and (Ab-Amylin) $A\beta_{15-40}|amylin_{15-35}$. The averages are over all three trajectories.

the course of the molecular dynamics trajectory. An internal water channel for the $A\beta$ is found in the vicinity of the loop region of the D_{23}−K_{28} salt-bridges (A_{21}, D_{23}, K_{28}, A_{30}, and I_{32}). On the other hand, the loop region in amylin formed by H_{18}−N_{23} is devoid of water molecules as was observed also in a recent simulation by Liang et al.[37] Our simulations show that water molecules enter into polar cavities (internal polar side chains or ionizable groups) around the polar amino acids N_{14}, L_{16}, S_{28}, and T_{30} (Figure 7) instead of the loop region of amylin, which is rich in hydrophobic amino acids. This is consistent with a recent study,[52] which showed that the water content in the protein interior can be modulated by the polarity of the protein cavity. The average number of internal waters differs for the three oligomers. We find about 30 molecules of water in $A\beta_{15-40}$, about 20 water molecules in $A\beta_{15-40}|amylin_{15-35}$ heteroassembly, but only around 15 water molecules in the $amylin_{15-35}$ oligomer.

dx.doi.org/10.1021/cn400141x | ACS Chem. Neurosci. 2013, 4, 1488−1500

The location in the β-strand−turn−β-strand motif, where water molecules are present, differs among the three octamers. In the Aβ octamer, water molecules are located around the loop region, while in amylin they are found in the middle of the two β-stands. This difference in the location of the water cavity determines the flow of the water molecules across the cross-seeded oligomer, especially at the border. Here, water coming from the loop region of Aβ encounters the hydrophobic loop region of amylin. Such interfacial interaction will affect the stability of strand-to-strand association at this particular location as is evident in the RMSF and SASA and hydrophobic contacts (Figure 3, Figure S1, Supporting Information, and Table 1, respectively). However, despite the difference in the location of hydration cavity in the heteroassembly, we observe still a flow of water molecules from one side into the other. This suggests flow of water and electrolyte through the pore as a possible common toxicity mechanism, because the stability of the oligomers in our simulations indicates that Aβ and amylin can cross-seed to form structures capable of inserting into membranes. Hence, our results suggest cross-sequence interaction between Aβ and amylin as the apparent link between Alzheimer's disease and type II diabetes.

CONCLUSIONS

We have reported results from long constant temperature molecular dynamics simulations of preformed octamers (amylin$_{10-35}$, Aβ_{15-40}, and a heteroassembly of both amylin$_{10-35}$ and Aβ_{15-40}) in explicit solvent. Our analysis shows that with the exception of the edge strands, the individual chains in all three octamers retain a β-strand−turn−β-strand motif under physiological conditions. Throughout the whole trajectories, the oligomers are characterized by close hydrophobic packing at the N-terminus, fluctuations in the loop region, moderate flexibility in the C-terminal region, and larger flexibility in the outer layer strands of Aβ_{15-40} and amylin$_{10-35}$ chains. All three octamers keep the network of hydrogen bonds and the interstrand and intrastrand hydrophobic contacts that stabilize the U-shaped start configurations. This highlights the importance of hydrophobic interactions and the highly organized interstrand hydrogen bonding in conferring stability to an octamer. Our results also demonstrate the need to monitor the underappreciated face-to-face hydrophobic interactions for probing dynamics in the internal structure. The distance between the two β-sheets is about 2 Å smaller in the amylin octamer than in the amylin strand at the interface between Aβ and amylin chains in the cross-seeded Aβ_{15-40}|amylin$_{10-35}$ octamers. This smaller distance indicates that the interaction of the two peptides at the interface requires structural flexibility and conformational adaptation for better shape complementarity. Note that despite their sequence dissimilarity the Aβ and amylin chains maintain even in the mixed Aβ_{15-40}|amylin$_{10-35}$ oligomer their initial U-shaped motif without distortion (except for the terminal strands 1 and 8). MM-PBSA calculations show that the Aβ_{15-40}|amylin$_{15-35}$, amylin$_{10-35}$, and Aβ_{15-40} octamers are favored over the corresponding systems of two separated tetramers by average interaction energies of −91.70, −127.16, and −131 (kcal/mol). Even accounting for limited accuracy of MM-PBSA calculations, these numbers show that lateral growth is favorable for both self- and cross-seeded oligomers. The favorable free energy of the cross-seeded oligomer results from changes in side-chain packing (as can be seen from the per residue decomposition of energy terms) in the flexible C-terminal region that allow the peptides at the border between Aβ and amylin chains to adopt configurations that stabilize the heteroassembly. Note that by design our stability analysis cannot give any information on whether Aβ seeds amylin or vice versa. According to Nuallian et al.,[16] Aβ fibrils seeded amylin efficiently but amylin was less efficient in seeding the growth of Aβ aggregates. Our simulations only indicate the stability of such aggregates that are also observed experimentally in the brain−blood vessel of both of demented diabetics and late onset Alzheimer's Disease nondiabetic patients.[20]

The characterization of toxic soluble oligomeric intermediates is a challenge because of their transient nature, small sizes, and heterogeneous morphologies.[53] Several structural models have been suggested for amyloid oligomers including annular or β-barrel,[53] cylindrin,[6] and parallel in-register β-sheet. Recent X-ray diffraction and electron microscopy studies evidenced that laterally associated fibril filaments of Aβ can wrap around forming a hole along the axis of assembly. All these models of amyloid-β fibrillar oligomers have in common that they form pore-like structures believed to be essential for their toxicity. Our recent simulations on small hydrophobic cylindrins revealed water molecules entering into the interior channel that might lead to leakage upon insertion into the membrane.[47] On the other hand, a recent study on the mechanism of membrane insertion of toxic fibrils like Aβ suggests that a U-shaped trimer is the minimum oligomer size for effective insertion to membrane and its toxicity.[54] Note that while a recent NMR study has reported partial helical structures for dissolved amylin peptides, these early helical intermediates convert into β structures upon binding to membrane.[55] Computational studies by Jang et al. of the interactions of lipid bilayer with preformed Aβ protofilaments[54] found U-shaped Aβ oligomers in both aqueous solution and membrane. Another simulation study[56] of Aβ-monomer and Aβ-dimers bound to a membrane model starting from an initial helical peptide conformation showed again β-hairpin motif formation. These studies suggest that Aβ aggregates in lipid bilayers adopt a structure similar to that in aqueous medium and especially that the U-shaped motif is preserved. In the present simulations, all three oligomers retain their fibril-like U-shaped structure, and water molecules are found to pass through hydration channels. In Aβ, these are located around the loop region, while in amylin, the water molecules are found in the middle of the two β-stands near a group of polar amino acids whose side chains point toward the interior of the oligomer cavity (N_{14}, S_{28}, and T_{30}). Despite the different locations of the hydration channels in Aβ_{15-40} octamers and amylin$_{10-35}$ octamers, we find a flow of internal water molecules from amylin$_{10-35}$ side into the Aβ_{15-40} in the cross-seeded Aβ_{15-40}|amylin$_{15-35}$ octamer.

The presence of a hydration cavity and the maintenance of U-shaped structure in by the fibril-like octamers suggest as a common toxicity mechanism, the leakage of water and electrolyte through the pore in the various assemblies of amyloid peptides, both homo-oligomers and cross-seeded hetero-oligomers. Our simulation indicates that the hydrophobic core comprising the β_1 and β_2 regions of the cross-seeded model is crucial for the stability and elongation of the aggregate. These regions should therefore be considered as potential targets for structure-based design of aggregation inhibitors.[57,58]

METHODS

Construction of the Fibril-like Oligomer Models. It is known from NMR studies that Aβ fibers of various Aβ oligomers[59] share a U-shaped motif where two β-strand segments (residues 10−24 and 30−40) are joined by a U-turn and stabilized by interior salt bridges between residues D_{23} and K_{28}.[60,42] Amylin has a similar β-strand−loop−β-strand motif, with the loop region located at residues 18−27 straddled by two β-strands comprising residues 8−17 and 28−37.[11] Since both Aβ and amylin fibril models contain this U-shaped motif, cross interaction is assumed to depend mostly on their β-strand domains,[61] and we use in the present study not the full-length peptides but truncated fragments that contain this motif. This is justified because residues 1−16 are disordered in Aβ_{1-42} fibrils and residues 1−9 in Aβ_{1-40} fibrils, and Takeda et al[50] found that the Aβ_{1-40} and Aβ_{10-40} systems are equivalent. Hence, we make in the present study the assumption that Aβ_{15-40} fibrils are similar to such of Aβ_{1-40} or Aβ_{10-40}. For amylin, residues 1−7 are not part of a β-sheet in the experimental structure, and because of a disulfide bridge between cysteine residues 2 and 7,[38] do not contribute to aggregate assembly. In order to ensure equal length of our molecules, we therefore used truncated Aβ_{15-40} and amylin$_{10-35}$ peptides (capped with acetyl and amide groups to mimic the full-length peptide) in the present study. The Aβ_{15-40} fibril model is derived from protofilament models of Aβ_{9-42} (http://people.mbi.ucla.edu/sawaya/jmol/fibrilmodels/), Colletier et al.,[62] after removing the residues 9−14 and residues 41−42. The amylin$_{10-35}$ fibril model is obtained in a similar manner from the model of amylin$_{1-37}$. Tetramers of these fragments were extracted from the fibril models of the Eisenberg group[38,62] and are used to construct Aβ_{15-40} octamers, amylin$_{10-35}$ octamers, and Aβ_{15-40}|amylin$_{10-35}$ octamer heteroassemblies, taking into consideration the interactions in the β-structure domain and ones that stabilize the U-turn, e.g., hydrophobic interactions, electrostatic interactions, polar interactions, and salt bridges. For building the Aβ_{15-40}|amylin$_{10-35}$ octamer heteroassembly, we align and superimpose the chains to maximize the overlap between the hydrophobic residues, the U turn, and the C-terminal and N-terminal regions. For example, hydrophobic residues in the $L_{13}ANFL_{17}$ motif of the β_1 region of amylin are matched with the hydrophobic residues $L_{17}VFFA_{21}$ in Aβ (Figure 1B), and the hydrophobic $A_{25}ILSS_{29}$ motif in the β_2 region of amylin is matched with the hydrophobic residues $A_{30}IIGL_{34}$ in the β_2 region of Aβ (Figure 1B). Face-to-face interactions between β-sheets, usually hydrophobic contacts, are common in amyloid structure, but their role in the formation and stabilization of amyloid fibrils has been underappreciated.[40,63] The U-shaped structures reveal such contact between residues V_{36}/L_{17}, L_{34}/F_{19}, and I_{32}/A_{21} of Aβ, T_{30}/N_{14}, S_{28}/L_{16}, and I_{26}/H_{18} for amylin (Figure 1C,D), and a combination of these face-to-face interactions in the Aβ_{15-40}|amylin$_{10-35}$ octamer heteroassembly.

Molecular Dynamics Simulations. Reliable simulations of structure and dynamics of large biomolecules require accurate and reliable force fields.[64] A common choice for exploring amyloid peptide aggregation[64,65] is the combination of the AMBER ff99SB force field[66] with explicit water (TIP3P)[67,68] used also in this study. We use the GROMACS program, version 4.5.3,[69] and a time step of 2 fs. Hydrogen atoms are added with the *pdb2gmx* module of the GROMACS suite. The start configurations of all proteins are set in the center of a cubic box where the distance between the solute and the edge of the box is at least 12 Å. Periodic boundary conditions are employed, and electrostatic interactions are calculated with the PME algorithm.[70,71] Hydrogen atoms are constrained with the LINCS[72] algorithm, while for water, the Settle algorithm is used.[73] The temperature of 310 K is kept constant by the Parrinello−Donadio−-Bussi algorithm[74] (τ = 0.1 fs), which is similar to Berendsen coupling but adds a stochastic term that ensures a proper canonical ensemble.[74,75] In a similar way, the pressure is kept constant at 1 bar by the Parrinello−Rahman algorithm[76] (τ = 1 fs). The temperature of 310 K is chosen as a compromise between preserving the experimentally observed stability of the amyloid fibrils[77] and the desire to enhance sampling by raising temperature.[78,79] The solvated start configuration is first energy minimized using the steepest descent method, followed by conjugate gradient. Afterward, the system is equilibrated in two steps of 500 ps, the first step in an *NVT* ensemble and the second phase in an *NPT* ensemble at 1 bar. After equilibrization, 300 ns of trajectories are analyzed for each system to examine the structural changes of the oligomer aggregates with time. Data are saved at 4.0 ps intervals for further analysis. For each system (solely Aβ_{15-40}, solely amylin$_{10-35}$, and mixed Aβ_{15-40}−amylin$_{10-35}$), we run three distinct simulations of 300 ns with different initial velocity distributions. This allows us to test that we reached equilibrium and guarantees three independent sets of measurements.

The molecular dynamics trajectories are analyzed with the tool set of the GROMACS package. Especially, we monitor conformational changes and stability of the oligomer models through the time evolution of the root mean square deviations of the Cα atoms (RMSD), root-mean-square fluctuation (RMSF), solvent accessible surface area (SASA), hydrophobic contact distances, hydrogen bonds, and D_{23}−K_{28} salt bridges, measured with the *g_hbond* and *g_dist* modules in GROMACS. Hydrogen bonds are defined by a distance cut off between donor and acceptor of 0.36 nm and an angle cut off of 30°. Configurations are visualized using PyMOL.[80]

Free Energy Calculations. The binding energy between the tetramers that form the octameric oligomers (Figure S4, Supporting Information) are estimated with the MM-PBSA methodology as implemented in AMBER11[81] using the same force field and water model as above. The free energy of a molecule in the MM-PBSA is computed as the sum of the molecular mechanics energy in the gas phase, the solvation free energy, and the conformational entropy. Conformational effects are taken into account by averaging over the ensemble of configuration as generated in the molecular dynamics simulations. From the free energies of tetramer 1 (A), tetramer 2 (B), and octamer complex (C), the binding free energy is computed by subtracting the first two from the latter one from a single simulation of the complex (Figure S4, Supporting Information).

$$\Delta G_{\text{binding}} = \langle G_C \rangle - \langle G_A \rangle - \langle G_B \rangle$$

The bracket $\langle\rangle$ indicates a trajectory average, and the free energy of each system X = A, B, or C is computed as a sum of the three terms:

$$\langle \Delta G_X \rangle = \langle E_{MM} \rangle + \langle \Delta G_{solv} \rangle - \langle T\Delta S \rangle$$

Here, the molecular mechanics energy, E_{MM}, is the sum of the internal energy (bonds, angles, and dihedrals; E_{int}), electrostatic energy (E_{ele}), and van der Waals term (E_{vdw}):

$$E_{MM} = E_{int} + E_{ele} + E_{vdw}$$

The solvation energy, ΔG_{solv}, can be divided into the polar and nonpolar part:

$$\Delta G_{solv} = \Delta G_{PB} + \Delta G_{SA}$$

where the polar part, ΔG_{PB}, describes the electrostatic contribution to solvation as obtained from Poisson−Boltzmann (PB) calculations in a continuum solvent model, and the nonpolar contribution, ΔG_{SA}, is proportional to the solvent accessible surface area (SASA):

$$\Delta G_{SA} = \gamma \text{SASA} + b$$

In our calculations, we use the AMBER11 default parameter for γ and b.

ASSOCIATED CONTENT

Supporting Information

System set up for binding free energy calculation and additional results on structural flexibility, hydrogen bond content, salt bridge stability, and electrostatic contributions to the binding free energy. This material is available free of charge via the Internet at http://pubs.acs.org.

AUTHOR INFORMATION

Corresponding Author

*Email: uhansmann@ou.edu.

Funding

We acknowledge support from the National Institutes of Health (Grant Number GM62838). This research used resources of the National Energy Research Scientific Computing Center, which is supported by the Office of Science of the U.S. Department of Energy under Contract No. DE-AC02-05CH11231. Parts of the simulations were done on the BOOMER cluster of the University of Oklahoma. F.Y. is supported by Hacetttepe University Scientific Research Fund under Project Number 012.D12.602.001.

Notes

The authors declare no competing financial interest.

ACKNOWLEDGMENTS

F.Y. thanks the Department of Chemistry and Biochemistry for kind hospitality during his sabbatical stay at the University of Oklahoma.

REFERENCES

(1) Stefani, M. (2012) Structural features and cytotoxicity of amyloid oligomers: Implications in Alzheimer's disease and other diseases with amyloid deposits. *Prog. Neurobiol. 99*, 226−245.

(2) Eisenberg, D., and Jucker, M. (2012) The Amyloid State of Proteins in Human Diseases. *Cell 148*, 1188−1203.

(3) Narayan, P., Ganzinger, K. A., McColl, J., Weimann, L., Meehan, S., Qamar, S., Carver, J. A., Wilson, M. R., George-Hyslop, P. S., Dobson, C. M., and Klenerman, D. (2013) Single Molecule Characterization of the Interactions between Amyloid-beta Peptides and the Membranes of Hippocampal Cells. *J. Am. Chem. Soc. 135*, 1491−1498.

(4) Bolognesi, B., Kumita, J. R., Barros, T. P., Esbjorner, E. K., Luheshi, L. M., Crowther, D. C., Wilson, M. R., Dobson, C. M., Favrin, G., and Yerbury, J. J. (2010) ANS Binding Reveals Common Features of Cytotoxic Amyloid Species. *ACS Chem. Biol. 5*, 735−740.

(5) Kayed, R., Head, E., Thompson, J. L., McIntire, T. M., Milton, S. C., Cotman, C. W., and Glabe, C. G. (2003) Common structure of soluble amyloid oligomers implies common mechanism of pathogenesis. *Science 300*, 486−489.

(6) Laganowsky, A., Liu, C., Sawaya, M. R., Whitelegge, J. P., Park, J., Zhao, M. L., Pensalfini, A., Soriaga, A. B., Landau, M., Teng, P. K., Cascio, D., Glabe, C., and Eisenberg, D. (2012) Atomic View of a Toxic Amyloid Small Oligomer. *Science 335*, 1228−1231.

(7) Wu, J. W., Breydo, L., Isas, J. M., Lee, J., Kuznetsov, Y. G., Langen, R., and Glabe, C. (2010) Fibrillar Oligomers Nucleate the Oligomerization of Monomeric Amyloid beta but Do Not Seed Fibril Formation. *J. Biol. Chem. 285*, 6071−6079.

(8) Liu C, Z. M., Jiang, L., Cheng, P. N., Park, J., Sawaya, M. R., Pensalfini, A., Gou, D., Berk, A. J., Glabe, C. G., Nowick, J., and Eisenberg, D. (2012) Out-of-register β-sheets suggest a pathway to toxic amyloid aggregates. *Proc. Natl. Acad. Sci. U.S.A. 109*, 20913.

(9) Ott, A., Stolk, R. P., van Harskamp, F., Pols, H. A. P., Hofman, A., and Breteler, M. M. B. (1999) Diabetes mellitus and the risk of dementia - The Rotterdam Study. *Neurology 53*, 1937−1942.

(10) Cheng, G., Huang, C., Deng, H., and Wang, H. (2012) Diabetes as a risk factor for dementia and mild cognitive impairment: A meta-analysis of longitudinal studies. *Intern. Med. J. 42*, 484−491.

(11) Janson, J., Laedtke, T., Parisi, J. E., O'Brien, P., Petersen, R. C., and Butler, P. C. (2004) Increased risk of type 2 diabetes in Alzheimer disease. *Diabetes 53*, 474−481.

(12) Zhang, Y., Zhou, B., Deng, B., Zhang, F., Wu, J. X., Wang, Y. G., Le, Y. Y., and Zhai, Q. W. (2013) Amyloid-beta Induces Hepatic Insulin Resistance In Vivo via JAK2. *Diabetes 62*, 1159−1166.

(13) Sato, N., and Morishita, R. (2013) Plasma A beta: A Possible Missing Link Between Alzheimer Disease and Diabetes. *Diabetes 62*, 1005−1006.

(14) Lorenzo, A., Razzaboni, B., Weir, G. C., and Yankner, B. A. (1994) Pancreatic-islet cell toxicity of amylin associated with type-2 diabetes-mellitus. *Nature 368*, 756−760.

(15) Hoppener, J. W. M., Ahren, B., and Lips, C. J. M. (2000) Islet amyloid and type 2 diabetes mellitus. *N. Engl. J. Med. 343*, 411−419.

(16) O'Nuallain, B., Williams, A. D., Westermark, P., and Wetzel, R. (2004) Seeding specificity in amyloid growth induced by heterologous fibrils. *J. Biol. Chem. 279*, 17490−17499.

(17) Andreetto, E., Yan, L. M., Tatarek-Nossol, M., Velkova, A., Frank, R., and Kapurniotu, A. (2010) Identification of Hot Regions of the A beta-IAPP Interaction Interface as High-Affinity Binding Sites in both Cross- and Self-Association. *Angew. Chem., Int. Ed. 49*, 3081−3085.

(18) Ida, N., Hartmann, T., Pantel, J., Schroder, J., Zerfass, R., Forstl, H., Sandbrink, R., Masters, C. L., and Beyreuther, K. (1996) Analysis of heterogeneous beta A4 peptides in human cerebrospinal fluid and blood by a newly developed sensitive Western blot assay. *J. Biol. Chem. 271*, 22908−22914.

(19) Banks, W. A., Kastin, A. J., Maness, L. M., Huang, W. T., and Jaspan, J. B. (1995) Permeability of the blood-brain-barrier to amylin. *Life Sci. 57*, 1993−2001.

(20) Jackson, K., Barisone, G. A., Diaz, E., Jin, L. W., DeCarli, C., and Despa, F. (2013) Amylin deposition in the brain: a second amyloid in Alzheimer's disease? *Annals of Neurology*, DOI: 10.1002/ana.23956.

(21) Lasagna-Reeves, C. A., Glabe, C. G., and Kayed, R. (2011) Amyloid-beta Annular Protofibrils Evade Fibrillar Fate in Alzheimer Disease Brain. *J. Biol. Chem. 286*, 22122−22130.

(22) Butterfield, S. M., and Lashuel, H. A. (2010) Amyloidogenic Protein Membrane Interactions: Mechanistic Insight from Model Systems. *Angew. Chem., Int. Ed. 49*, 5628−5654.

(23) Matthes, D., Gapsys, V., and de Groot, B. L. (2012) Driving Forces and Structural Determinants of Steric Zipper Peptide Oligomer Formation Elucidated by Atomistic Simulations. *J. Mol. Biol. 421*, 390−416.

(24) Straub, J. E., and Thirumalai, D. (2011) Toward a Molecular Theory of Early and Late Events in Monomer to Amyloid Fibril Formation. In *Annual Review of Physical Chemistry* (Leone, S. R., Cremer, P. S., Groves, J. T., and Johnson, M. A., Eds.), Vol *62*, pp 437−463, Annual Reviews, Palo Alto, CA.

(25) Han, M., and Hansmann, U. H. E. (2011) Replica exchange molecular dynamics of the thermodynamics of fibril growth of Alzheimer's A beta(42) peptide. *J. Chem. Phys. 135*, No. 065101.

(26) Reddy, G., Straubb, J. E., and Thirumalai, D. (2009) Dynamics of locking of peptides onto growing amyloid fibrils. *Proc. Natl. Acad. Sci. U. S. A. 106*, 11948−11953.

(27) Xi, W. H., Li, W. F., and Wang, W. (2012) Template Induced Conformational Change of Amyloid-beta Monomer. *J. Phys. Chem. B 116*, 7398−7405.

(28) Tseng, B. P., Esler, W. P., Clish, C. B., Stimson, E. R., Ghilardi, J. R., Vinters, H. V., Mantyh, P. W., Lee, J. P., and Maggio, J. E. (1999) Deposition of monomeric, not oligomeric, A beta mediates growth of Alzheimer's disease amyloid plaques in human brain preparations. *Biochemistry 38*, 10424−10431.

(29) Miller, Y., Ma, B. Y., and Nussinov, R. (2011) Synergistic Interactions between Repeats in Tau Protein and A beta Amyloids May Be Responsible for Accelerated Aggregation via Polymorphic States. *Biochemistry 50*, 5172−5181.

(30) Ma, B. Y., and Nussinov, R. (2012) Selective Molecular Recognition in Amyloid Growth and Transmission and Cross-Species Barriers. *J. Mol. Biol. 421*, 172−184.

(31) Dessalew, N., and Mikre, W. (2008) On the paradigm shift towards multitarget selective drug design. *Curr. Comput.-Aided Drug Des. 4*, 76−90.

(32) Hopkins, A. L. (2008) Network pharmacology: The next paradigm in drug discovery. *Nat. Chem. Biol. 4*, 682−690.

(33) Sarell, C. J., Woods, L. A., Su, Y. C., Debelouchina, G. T., Ashcroft, A. E., Griffin, R. G., Stockley, P. G., and Radford, S. E. (2013) Expanding the Repertoire of Amyloid Polymorphs by Co-polymerization of Related Protein Precursors. *J. Biol. Chem. 288*, 7327−7337.
(34) Makarava, N., Ostapchenko, V. G., Savtchenko, R., and Baskakov, I. V. (2009) Conformational Switching within Individual Amyloid Fibrils. *J. Biol. Chem. 284*, 14386−14395.
(35) Dobson, C. M. (1999) Protein misfolding, evolution and disease. *Trends Biochem. Sci. 24*, 329−332.
(36) Knowles, T. P., Fitzpatrick, A. W., Meehan, S., Mott, H. R., Vendruscolo, M., Dobson, C. M., and Welland, M. E. (2007) Role of intermolecular forces in defining material properties of protein nanofibrils. *Science 318*, 1900−1903.
(37) Liang, G. Z., Zhao, J., Yu, X., and Zheng, J. (2013) Comparative Molecular Dynamics Study of Human Islet Amyloid Polypeptide (IAPP) and Rat IAPP Oligomers. *Biochemistry 52*, 1089−1100.
(38) Wiltzius, J. J. W., Sievers, S. A., Sawaya, M. R., Cascio, D., Popov, D., Riekel, C., and Eisenberg, D. (2008) Atomic structure of the cross-beta spine of islet amyloid polypeptide (amylin). *Protein Sci. 17*, 1467−1474.
(39) Zhao, J. H., Liu, H. L., Liu, Y. F., Lin, H. Y., Fang, H. W., Ho, Y., and Tsai, W. B. (2009) Molecular Dynamics Simulations to Investigate the Aggregation Behaviors of the A beta(17−42) Oligomers. *J. Biomol. Struct. Dyn. 26*, 481−490.
(40) Pin-Nan Cheng, J. D. P., and Nowick, J. S. (2013) The Supramolecular Chemistry of β-Sheets. *J. Am. Chem. Soc. 135*, 5477−5492.
(41) Sawaya, M. R., Sambashivan, S., Nelson, R., Ivanova, M. I., Sievers, S. A., Apostol, M. I., Thompson, M. J., Balbirnie, M., Wiltzius, J. J. W., McFarlane, H. T., Madsen, A. O., Riekel, C., and Eisenberg, D. (2007) Atomic structures of amyloid cross-beta spines reveal varied steric zippers. *Nature 447*, 453−457.
(42) Petkova, A. T., Yau, W. M., and Tycko, R. (2006) Experimental constraints on quaternary structure in Alzheimer's beta-amyloid fibrils. *Biochemistry 45*, 498−512.
(43) Buchete, N. V., Tycko, R., and Hummer, G. (2005) Molecular dynamics simulations of Alzheimer's beta-amyloid protofilaments. *J. Mol. Biol. 353*, 804−821.
(44) Homeyer, N., and Gohlke, H. (2012) Free Energy Calculations by the Molecular Mechanics Poisson-Boltzmann Surface Area Method. *Mol. Inf. 31*, 114−122.
(45) Berhanu, W. M., and Masunov, A. E. (2011) Molecular Dynamic Simulation of Wild Type and Mutants of the Polymorphic Amyloid NNQNTF Segments of Elk Prion: Structural Stability and Thermodynamic of Association. *Biopolymers 95*, 573−590.
(46) Gohlke, H., and Case, D. A. (2004) Converging free energy estimates: MM-PB(GB)SA studies on the protein-protein complex Ras-Raf. *J. Comput. Chem. 25*, 238−250.
(47) Workalemahu, M., and Berhanu, U. H. E. H. (2013) The stability of cylindrin β-barrel amyloid oligomer models − a molecular dynamics study. *Proteins 81*, 1542−1555.
(48) Park, J., Kahng, B., and Hwang, W. (2009) Thermodynamic Selection of Steric Zipper Patterns in the Amyloid Cross-beta Spine. *PLoS Comput. Biol. 5*, No. e1000492.
(49) Liu, F. F., Liu, Z., Bai, S., Dong, X. Y., and Sun, Y. (2012) Exploring the inter-molecular interactions in amyloid-beta protofibril with molecular dynamics simulations and molecular mechanics Poisson-Boltzmann surface area free energy calculations. *J. Chem. Phys. 136*, No. 145101.
(50) Takeda, T., and Klimov, D. K. (2009) Probing the Effect of Amino-Terminal Truncation for A beta(1−40) Peptides. *J. Phys. Chem. B 113*, 6692−6702.
(51) Zheng, J., Jang, H., Ma, B., Tsai, C. J., and Nussinov, R. (2007) Modeling the Alzheimer A beta(17−42) fibril architecture: Tight intermolecular sheet-sheet association and intramolecular hydrated cavities. *Biophys. J. 93*, 3046−3057.
(52) Damjanovic, A., Schlessman, J. L., Fitch, C. A., Garcia, A. E., and Garcia-Moreno, B. (2007) Role of flexibility and polarity as determinants of the hydration of internal cavities and pockets in proteins. *Biophys. J. 93*, 2791−2804.
(53) Stroud, J. C., Liu, C., Teng, P. K., and Eisenberg, D. (2012) Toxic fibrillar oligomers of amyloid-beta have cross-beta structure. *Proc. Natl. Acad. Sci. U. S. A. 109*, 7717−7722.
(54) Jang, H., Connelly, L., Arce, F. T., Ramachandran, S., Kagan, B. L., Lal, R., and Nussinov, R. (2013) Mechanisms for the Insertion of Toxic, Fibril-like beta-Amyloid Oligomers into the Membrane. *J. Chem. Theory Comput. 9*, 822−833.
(55) Nanga, R. P. R., Brender, J. R., Vivekanandan, S., and Ramamoorthy, A. (2011) Structure and membrane orientation of IAPP in its natively amidated form at physiological pH in a membrane environment. *Biochim. Biophys. Acta, Biomembr. 1808*, 2337−2342.
(56) Manna, M., and C, M. (2013) Binding, Conformational Transition and Dimerization of Amyloid-b Peptide on GM1-Containing Ternary Membrane: Insights from Molecular Dynamics Simulation. *PLoS One 8*, No. e71308.
(57) Sievers, S. A., Karanicolas, J., Chang, H. W., Zhao, A., Jiang, L., Zirafi, O., Stevens, J. T., Munch, J., Baker, D., and Eisenberg, D. (2011) Structure-based design of non-natural amino-acid inhibitors of amyloid fibril formation. *Nature 475*, 96−100.
(58) Zheng, J., Liu, C., Sawaya, M. R., Vadla, B., Khan, S., Woods, R. J., Eisenberg, D., Goux, W. J., and Nowick, J. S. (2012) Macrocyclic β-Sheet Peptides That Inhibit the Aggregation of a Tau-Protein-Derived Hexapeptide. *J. Am. Chem. Soc. 134*, 17832−17832.
(59) Ono, K., Condron, M. M., and Teplow, D. B. (2009) Structure-neurotoxicity relationships of amyloid beta-protein oligomers. *Proc. Natl. Acad. Sci. U. S. A. 106*, 14745−14750.
(60) Luhrs, T., Ritter, C., Adrian, M., Riek-Loher, D., Bohrmann, B., Doeli, H., Schubert, D., and Riek, R. (2005) 3D structure of Alzheimer's amyloid-beta(1−42) fibrils. *Proc. Natl. Acad. Sci. U. S. A. 102*, 17342−17347.
(61) Raz, Y., and Y, M. (2013) Interactions between Aβ and Mutated Tau Lead to Polymorphism and Induce Aggregation of Aβ-Mutated Tau Oligomeric Complexes. *PLoS ONE 8*, No. e73303.
(62) Colletier, J. P., Laganowsky, A., Landau, M., Zhao, M. L., Soriaga, A. B., Goldschmidt, L., Flot, D., Cascio, D., Sawaya, M. R., and Eisenberg, D. (2011) Molecular basis for amyloid-beta polymorphism. *Proc. Natl. Acad. Sci. U. S. A. 108*, 16938−16943.
(63) Takeda, T., and Klimov, D. K. (2009) Probing Energetics of A beta Fibril Elongation by Molecular Dynamics Simulations. *Biophys. J. 96*, 4428−4437.
(64) Berhanu, W. M., and Hansmann, U. H. E. (2012) Structure and Dynamics of Amyloid-b Segmental Polymorphisms. *PLoS ONE 7*, No. e41479.
(65) Ndlovu, H., Ashcroft, A. E., Radford, S. E., and Harris, S. A. (2012) Effect of Sequence Variation on the Mechanical Response of Amyloid Fibrils Probed by Steered Molecular Dynamics Simulation. *Biophys. J. 102*, 587−596.
(66) Hornak, V., Abel, R., Okur, A., Strockbine, B., Roitberg, A., and Simmerling, C. (2006) Comparison of multiple amber force fields and development of improved protein backbone parameters. *Proteins 65*, 712−725.
(67) Zachariae, U., Schneider, R., Briones, R., Gattin, Z., Demers, J. P., Giller, K., Maier, E., Zweckstetter, M., Griesinger, C., Becker, S., Benz, R., de Groot, B. L., and Lange, A. (2012) beta-Barrel Mobility Underlies Closure of the Voltage-Dependent Anion Channel. *Structure 20*, 1540−1549.
(68) Kutzner, C., Grubmuller, H., de Groot, B. L., and Zachariae, U. (2011) Computational Electrophysiology: The Molecular Dynamics of Ion Channel Permeation and Selectivity in Atomistic Detail. *Biophys. J. 101*, 809−817.
(69) Pronk, S., Páll, S., Schulz, R., Larsson, P., Bjelkmar, P., Apostolov, R., Shirts, M. R., Smith, J. C., Kasson, P M., van der Spoel, D., Hess, B., and Lindahl, E. (2013) GROMACS 4.5: a high-throughput and highly parallel open source molecular simulation toolkit. *Bioinformatics 29*, 845−854.

(70) Darden, T., York, D., and Pedersen, L. (1993) Particle mesh ewald - an n. log(n) method for ewald sums in large systems. *J. Chem. Phys. 98*, 10089−10092.
(71) Essmann, U., Perera, L., Berkowitz, M. L., Darden, T., Lee, H., and Pedersen, L. G. (1995) A smooth particle mesh ewald method. *J. Chem. Phys. 103*, 8577−8593.
(72) Hess, B. (2008) P-LINCS: A parallel linear constraint solver for molecular simulation. *J. Chem. Theory Comput. 4*, 116−122.
(73) Miyamoto, S., and Kollman, P. A. (1992) Settle - an analytical version of the shake and rattle algorithm for rigid water models. *J. Comput. Chem. 13*, 952−962.
(74) Bussi, G., Donadio, D., and Parrinello, M. (2007) Canonical sampling through velocity rescaling. *J. Chem. Phys. 126*, No. 014101.
(75) Bussi, G., Zykova-Timan, T., and Parrinello, M. (2009) Isothermal-isobaric molecular dynamics using stochastic velocity rescaling. *J. Chem. Phys. 130*, No. 074101.
(76) Parrinello, M., and Rahman, A. (1981) Polymorphic transitions in single-crystals - a new molecular-dynamics method. *J. Appl. Phys. 52*, 7182−7190.
(77) Meersman, F., and Dobson, C. M. (2006) Probing the pressure-temperature stability of amyloid fibrils provides new insights into their molecular properties. *Biochim. Biophys. Acta 1764*, 452−460.
(78) Berhanu, W. M., and Masunov, A. E. (2012) Controlling the aggregation and rate of release in order to improve insulin formulation: molecular dynamics study of full-length insulin amyloid oligomer models. *J. Mol. Model. 18*, 1129−1142.
(79) Berhanu, W. M., and Masunov, A. E. (2012) Unique example of amyloid aggregates stabilized by main chain H-bond instead of the steric zipper: Molecular dynamics study of the amyloidogenic segment of amylin wild-type and mutants. *J. Mol. Model. 18*, 891−903.
(80) DeLano, W. L. (2002) *PyMOL molecular graphics system*, version 1.3.0.4, Schrödinger, LLC.
(81) Miller, B. R., McGee, T. D., Swails, J. M., Homeyer, N., Gohlke, H., and Roitberg, A. E. (2012) MMPBSA.py: An Efficient Program for End-State Free Energy Calculations. *J. Chem. Theory Comput. 8*, 3314−3321.